

## Electronic supplementary information for: ‘Comparing the ultraviolet photostability of azole chromophores’

Gareth M. Roberts, Craig A. Williams, Martin J. Paterson, Susanne Ullrich and Vasilios G. Stavros\*

\*To whom correspondence should be addressed: v.stavros@warwick.ac.uk

### 1. Experiment details

Time-resolved velocity map imaging (VMI) experiments utilize femtosecond (fs) laser pulses derived from a commercial Ti:Sapphire oscillator and regenerative amplifier system (Spectra-Physics, Tsunami and Spitfire XP, respectively). The regenerative amplifier operates at 125 Hz for these experiments and delivers 3 mJ/pulse centered at 800 nm with a temporal full width at half maximum (FWHM) of 45 fs. These fundamental pulses have a bandwidth of ~30 nm ( $\sim 500 \text{ cm}^{-1}$ ). The fundamental output is subsequently split into three beams of equal energy (1 mJ/pulse). Of these three beams, one is up-converted into the 200 nm pump, which is achieved *via* frequency doubling the fundamental in a type-I  $\beta$ -barium borate (BBO) crystal to generate 400 nm, followed by successive frequency mixing (type-II and type-I BBO crystals, respectively) with the residual 800 nm pulses to generate third harmonic (267 nm) and finally the desired 200 nm fourth harmonic (~1  $\mu\text{J}/\text{pulse}$ ). The remaining two beams are used to pump two optical parametric amplifiers (Light Conversion, TOPAS model 4/800/f), of which one is used in these experiments to generate 243.1 nm probe pulses (~7  $\mu\text{J}/\text{pulse}$ ). These 243.1 nm probe pulses are used to selectively ionize any H-atoms *via* a [2 + 1] resonance enhanced multiphoton ionization (REMPI) process, resonant with the two-photon allowed  $2\text{s} \leftarrow 1\text{s}$  transition. The temporal delay between pump and probe pulses ( $\Delta t$ ) is controlled by passing the 800 nm seed beam for the harmonic generation stage through a protected-gold hollow retro-reflector mounted on a computer controlled delay stage (Physik-Instrumente, M-505.4DG), providing a minimum step size for these experiments of 25 fs. Both pump and probe pulses are focused through  $f = 50 \text{ cm}$   $\text{MgF}_2$  and  $\text{CaF}_2$  lenses, respectively, and are collinearly recombined at a dichroic mirror. These collinearly focused beams then enter the interaction region of a VMI spectrometer where they perpendicularly intersect a molecular beam pulse of imidazole or pyrazole. Non-resonant multiphoton ionization of  $\text{NH}_3$  and Xe is employed as a method for determining both the delay position corresponding to the temporal overlap of the pump and probe ( $\Delta t = 0$ ), to within an accuracy of  $\pm 15$  fs, and the associated cross-correlation/instrument response function (IRF). For these experiments a Gaussian IRF is measured with a FWHM of ~160 fs.

Molecular beam pulses are generated by seeding imidazole or pyrazole (Sigma-Aldrich, > 98 %) molecules in helium (~2 bar) and transferred into vacuum using an Even-Lavie pulsed solenoid valve<sup>1</sup> operating at 125 Hz and synchronized to the laser system. The valve is heated to 100 °C in order to generate a sufficient vapor pressure of seed molecules. The backing pressure and opening time of the valve has been optimized to reduce the degree of clustering of the parent ion relative to the parent ion monomer. A typical opening time for the valve is ~13  $\mu\text{s}$ . The molecular beam machine consists of differentially pumped source and interaction chambers, partitioned by a 2 mm skimmer. The pulsed valve is housed within the source chamber, whilst the interaction chamber contains VMI optics, replicating the arrangement described by Eppink and Parker.<sup>2</sup> Generated cations are then accelerated

towards a position sensitive detector (under VMI focusing conditions) which consists of a pair of 40 mm diameter chevron microchannel plates (MCPs) coupled to a P-43 phosphor screen (Photek, VID-240). A timed voltage pulse (Behlke) is applied to the rear MCP to gate the detector for measuring only the  $H^+$  or  $D^+$  signal. A two-dimensional projection of the three-dimensional ion distribution is subsequently obtained by capturing the light emitted from the phosphor screen using a charge-coupled device (Foculus). One-dimensional radial/velocity spectra of the REMPI probed H or D atoms ( $H^+$  or  $D^+$ ) are obtained through deconvolution of the recorded  $H^+$  or  $D^+$  images by incorporating a polar onion-peeling method<sup>3</sup> into our data acquisition program coded in LabVIEW.

## 2. Preparation of deuterated isotopomers

### 2.1 $d_1$ isotopomers

Imidazole- $d_1$  and pyrazole- $d_1$  were prepared by dissolving ~2 g of imidazole or pyrazole (Sigma-Aldrich, > 98 %) in ~50 ml of  $D_2O$ . These solutions were then heated under reflux conditions in the presence of a small amount of 2 M NaOH (< 1 ml) for ~2 hours and the resulting  $d_1$  isotopomer products then recrystallized.

### 2.2 Pyrazole- $d_3$

Pyrazole- $d_3$  was prepared in a similar manner to the method described in ref. 4. Approximately 1 g of pyrazole (Sigma-Aldrich, > 98 %) was partially dissolved in ~10 ml of  $D_2O$ . The pyrazole solution was heated in an oven at 240 °C within a high pressure vessel (consisting of a Teflon container embedded in a stainless steel canister) for 48 hours to generate fully deuterated pyrazole (pyrazole- $d_4$ ). The resulting pyrazole- $d_4$  was recrystallized and then dissolved in ~20 ml of deionized  $H_2O$ , in addition to a small quantity of 2 M NaOH (< 1 ml). This solution was then heated under reflux conditions for a further 2 hours. The resultant pyrazole- $d_3$  products were finally recrystallized.

### 2.3 Mass spectra of isotopomers

The relative purities of the isotopomer products were assessed with laser induced time-of-flight (TOF) mass spectrometry, using the same experimental apparatus described above and in the main text of the edge article. These mass spectra are provided below in Figs. S1 – S3.

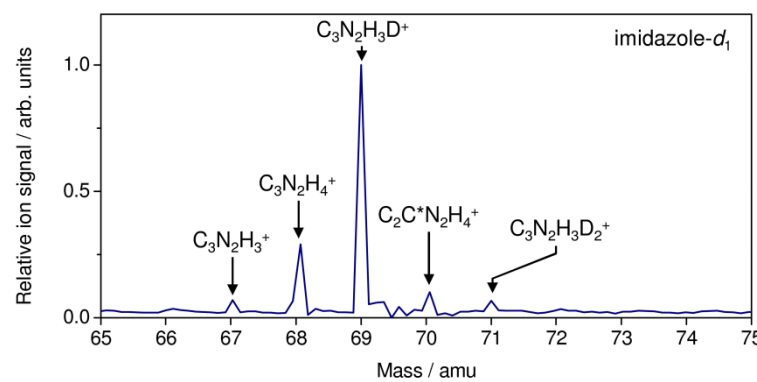


**Fig. S1** Laser induced TOF mass spectrum for imidazole- $d_1$ . The prominent peak at 69 amu corresponds to the imidazole- $d_1$  cation. Proposed (major) contributions to additional peaks are also given ( $C^* = C^{13}$ ).

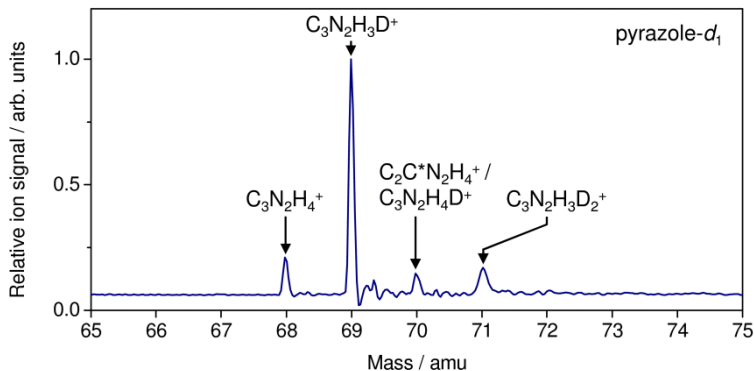


**Fig. S2** Laser induced TOF mass spectrum for pyrazole- $d_1$ . The prominent peak at 69 amu corresponds to the pyrazole- $d_1$  cation. Proposed (major) contributions to additional peaks are also given ( $C^* = C^{13}$ ).

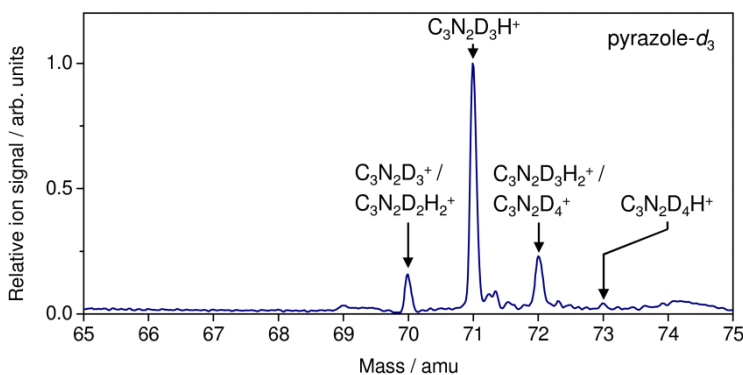


**Fig. S3** Laser induced TOF mass spectrum for pyrazole- $d_3$ . The prominent peak at 71 amu corresponds to the pyrazole- $d_3$  cation. Proposed (major) contributions to additional peaks are also given.

### 3. $H^+$ signal transients of high kinetic energy features

Transients of the high kinetic energy (KE) features with Gaussian profiles in the total kinetic energy release (TKER) spectra for imidazole (main text, Fig. 3(a)) and pyrazole (main text, Fig. 3(b)) are presented below in Fig. S4, up to a pump-probe delay of 600 ps. Both of these features are assigned to ultrafast (< 80 fs) H-atom elimination via  ${}^1\pi\sigma^*$  states, as described in the main text.

The high KE  $H^+$  signal transient for imidazole (Fig. S4(a)) does not display any additional signal increase by 600 ps, in line with ultrafast dynamics that are over by  $\sim$ 300 fs (see early time transients in ref. 5).

The analogous transient for pyrazole (Fig. S4(b)) displays a minor depletion in  $H^+$  signal out to 600 ps. We attribute this to the fact that at early pump-probe delays (< 1 ps), the high KE tail of the ‘Boltzmann-like’ feature (peaking at low KEs) is notably convoluted into the signal integrals of the high KE feature (see ref. 6), while at longer times the overall profile of the ‘Boltzmann-like’ distribution has changed such that there is less signal associated with this feature convoluted into the integrals of high KE signal (see Fig. 3(b) of the main text); this interpretation is also supported by comparing the H-atom TKER spectral profile for pyrazole- $d_1$  at 2.5 ps and 600 ps (Fig. 5(a), main text). This ultimately results in a small depletion in signal at longer pump-probe delays in the high KE signal transient for pyrazole.

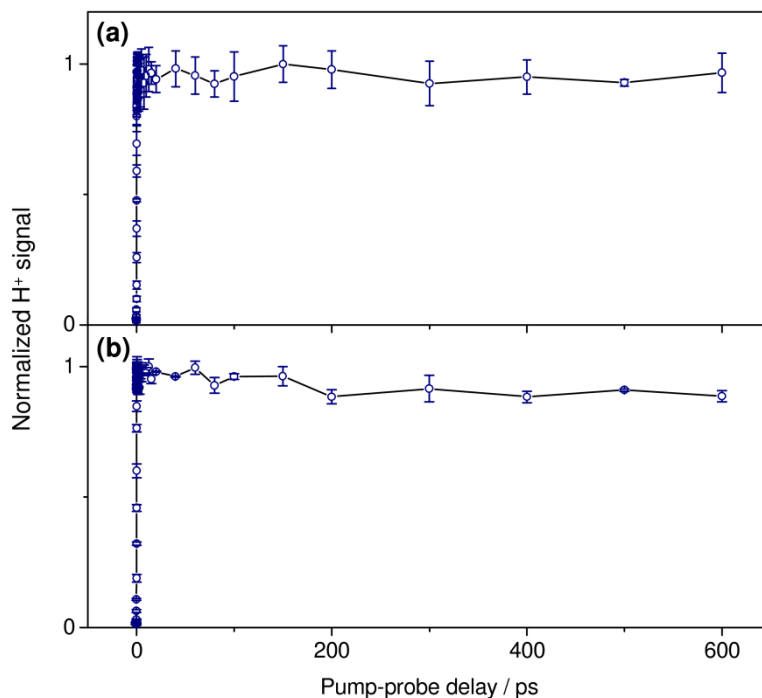


**Fig. S4** High kinetic energy H<sup>+</sup> signal transients obtained for (a) imidazole and (b) pyrazole. Transients are generated by integrating H<sup>+</sup> signal in the recorded TKER spectrum over an energy window of 8000 – 11500 cm<sup>-1</sup>, at each pump-probe delay.

#### 4. Fitting H<sup>+</sup> signal transients

H<sup>+</sup> signal transients for the low KE features are generated by integrating the signal over 200 – 1000 cm<sup>-1</sup> energy windows at each pump-probe delay. For imidazole and pyrazole-*d*<sub>3</sub>, transients are fitted using a combination of: (i) a fast exponential rise,  $r_1(\Delta t)$ , which describes the rapid rise in signal around  $\Delta t = 0$  ps attributed to probed H-atoms generated from multiphoton processes; and (ii) a second exponential rise function,  $r_2(\Delta t)$ , with a longer time constant to model the appearance of probed H-atoms generated through slower statistical dissociation processes. These two functions are each convoluted with the Gaussian instrument response function,  $g(\Delta t)$ , and have the form:

$$r_n(\Delta t) = g(\Delta t) * \left[ A_n \exp\left(-\frac{\Delta t}{\tau_n}\right) \right], \quad (\text{S1})$$

where  $A_n$  and  $\tau_n$  are the amplitudes and time constants associated with exponential rise function  $n$  and  $\Delta t$  is the pump-probe delay. The overall fit equation,  $f(\Delta t)$ , is subsequently given as

$$f(\Delta t) = r_1(\Delta t) + r_2(\Delta t). \quad (\text{S2})$$

The low KE H<sup>+</sup> transients obtained for pyrazole and pyrazole-*d*<sub>1</sub> are fitted using a modified version of eqn (S2):

$$\tilde{f}(\Delta t) = d(\Delta t) + r_1(\Delta t) + r_2(\Delta t), \quad (\text{S3})$$

where  $d(\Delta t)$  is an exponential decay function accounting for the rapidly decaying H<sup>+</sup> signal spike observed at  $\Delta t = 0$  ps in the low KE transients for these two species. The function  $d(\Delta t)$  is formally described as

$$d(\Delta t) = g(\Delta t) * \left[ 1 - B \exp\left(-\frac{\Delta t}{\tau_d}\right) \right]. \quad (\text{S4})$$

In eqn (S4),  $B$  is the amplitude of the decay function and  $\tau_d$  is the associated decay time constant.

## 5. Extracting branching ratios for N-H and C-H bond fission

Probed statistical H-atom signal contributions to the low KE featured in undeuterated pyrazole from N-H fission,  $A_{\text{NH}}$ , and C-H fission,  $A_{\text{CH}}$ , are obtained from measurements on deuterated isotopomers using the following expressions:

$$\begin{aligned} A_{\text{NH}} &= \frac{I_{\text{D}}}{I_{\text{D}} + I_{\text{H}}}, \\ A_{\text{CH}} &= \frac{I_{\text{H}}}{I_{\text{D}} + I_{\text{H}}} \end{aligned} \quad (\text{S5})$$

where

$$\begin{aligned} I_{\text{H}} &= I_{\text{H}}^{600} - I_{\text{H}}^{2.5} \\ I_{\text{D}} &= I_{\text{D}}^{600} - I_{\text{D}}^{2.5} \end{aligned} \quad (\text{S6})$$

Eqns. (S5) and (S6) consider the example case for pyrazole-*d*<sub>1</sub>. In eqn (S6),  $I_{\text{H}}^{600}$  and  $I_{\text{D}}^{600}$  are the integrated signal counts at low KEs (over 200 - 1000 cm<sup>-1</sup>) in the TKER spectrum derived from the H<sup>+</sup> velocity map image (resulting from C-H fission only) and a TKER spectrum derived from the D<sup>+</sup> velocity map image (resulting from N-D fission only; see Fig. 6(a) of main text of edge article), for pyrazole-*d*<sub>1</sub> at  $\Delta t = 600$  ps, respectively.  $I_{\text{H}}^{2.5}$  and  $I_{\text{D}}^{2.5}$  are the analogous integrals from the H<sup>+</sup> and D<sup>+</sup> derived TKER spectra, respectively, at  $\Delta t = 2.5$  ps and account for the fractions of signal at low KE associated with rapid multiphoton processes. An analogous approach to eqns. (S5) and (S6) have also been implemented to extract values for  $A_{\text{NH}}$  and  $A_{\text{CH}}$  from H<sup>+</sup> and D<sup>+</sup> derived TKER spectra obtained through measurements on pyrazole-*d*<sub>3</sub>.

## 6. RRKM theory calculations

RRKM calculations have been performed to predict the rate of unimolecular N-H bond fission,  $k_{\text{uni}}$ , from a vibrationally hot S<sub>0</sub> state in imidazole and pyrazole, using the standard rate equation:<sup>7</sup>

$$k_{\text{uni}} = \frac{1}{h} \frac{G^*(E - E_0)}{\rho(E)}. \quad (\text{S7})$$

In eqn (S7)  $h$  is Planck's constant,  $E$  is the internal energy available to the system,  $E_0$  is the transition state energy,  $G^*(E - E_0)$  is the number of vibrational states available at the transition state and  $\rho(E)$  is the density of vibrational states in  $S_0$ . A direct counts Beyer-Swinehart algorithm is used to calculate the density of vibrational states. Calculated anharmonic vibrational frequencies for imidazole and pyrazole in  $S_0$  are obtained from refs. 8 and 9, respectively; frequency calculations were performed at the B3LYP/6-311++G(d,p) level of theory. At the transition state, taken as the  ${}^1\pi\sigma^*/S_0$  conical intersection along the N-H coordinate, the disappearing modes (N-H stretch, in-plane N-H wag, and out-of-plane N-H wag) were all assumed to have half of their original frequencies at the equilibrium geometry in  $S_0$ . The available energy,  $E$ , for the calculations was set to  $50000\text{ cm}^{-1}$  (200 nm), while the critical energies,  $E_0$ , were taken to be  $34000\text{ cm}^{-1}$  and  $38000\text{ cm}^{-1}$  for imidazole and pyrazole, respectively.

## 7. *Ab initio* calculations

Complete active space self consistent field (CASSCF) methods are utilized to gain some insight into CI regions of the multi-dimensional potential energy surfaces where non-adiabatic dynamics are most probable in pyrazole. We highlight that this method generates qualitatively correct wavefunctions in regions of strong non-adiabatic coupling (*i.e.* CIs). CASSCF calculations are performed with the Gaussian 03 computational suite,<sup>10</sup> using a 6-31+G(d) Pople basis set. Initial starting geometries for CASSCF calculations in the ground state were obtained using density functional theory at the B3LYP/6-31G(d) level. The geometry minimum of the ground state is determined using a 6 electrons in 5 orbitals (6,5) active space consisting of the three  $\pi$  orbitals and the two  $\pi^*$  orbitals, which results in 50 singlet configuration functions. All calculations involving excited states are performed using a larger (10,8) active space, which includes the three  $\pi$  orbitals and the two  $\pi^*$  orbitals, in addition to the nitrogen lone pair (n orbital), the N-H  $\sigma$  orbital and the associated N-H  $\sigma^*$  orbital. This larger active space leads to 1176 singlet state configurations. All CI searches were performed without solving the orbital rotation derivatives in the couple perturbed multi-configurational self consistent field (CPMCSCF) equations.

Following excitation at 200 nm, population in the excited states may relax back to  $S_0$  via CIs, such as the representative pathway in Fig. 2(b) of the main edge article, which is accessible in both species. In addition to this relaxation trajectory, there may be other CIs with  $S_0$  which can be accessed along other nuclear coordinates of the potential energy landscape. For imidazole, Barbatti and co-workers have previously reported such CIs, and have shown that in addition of the  ${}^1\pi\sigma^*/S_0$  CI, the optically bright  ${}^1\pi\pi^*$  state also exhibits CIs with  $S_0$  which can be accessed along out-of-plane ring distortion modes.<sup>11</sup> However, relaxation pathways and regions of strong non-adiabatic coupling (*i.e.* CIs) in pyrazole's potential energy landscape have been explored less widely; hence, we have performed *ab initio* calculations using CASSCF methods to investigate excited state/ $S_0$  CIs in pyrazole, which may subsequently yield vibrationally hot pyrazole molecules in  $S_0$ .

With reference to Fig. S5(a), following excitation at 200 nm into the first  ${}^1\pi\pi^*$  state CASSCF results reveal that it may be feasible for population imparted to this state to relax back to  $S_0$  along a  ${}^1\pi\pi^*/S_0$  CI, the minimum energy crossing point (MECP) geometry of which is labeled accordingly. This CI may be accessed through a ring distortion coordinate. The two branching space modes, which are responsible for lifting the energetic degeneracy between the  ${}^1\pi\pi^*$  and  $S_0$  states at this MECP,<sup>12</sup> are presented in Fig. S5(b). These nuclear motions, assigned as the gradient difference (GD) and the

derivative coupling (DC), correspond to the gradient of the energy difference between the two electronic states around the CI and the derivative coupling parallel to the non-adiabatic coupling vector, respectively.<sup>12</sup> The latter motion is typically responsible for promoting population transfer between the two electronic surfaces, in this case  $^1\pi\pi^* \rightarrow S_0$ . We highlight that these calculations provide no insight into the topography of the  $^1\pi\pi^*$  state along the reaction coordinate towards the  $^1\pi\pi^*/S_0$  CI. There may be an energetic barrier to accessing the  $^1\pi\pi^*/S_0$  MECP geometry, although comparison with calculations of  $^1\pi\pi^*/S_0$  CIs in imidazole, tentatively suggest that this could be a barrierless relaxation channel to  $S_0$ .<sup>11</sup> Furthermore, the branching fraction for population transferred into a hot  $S_0$  state *via* the  $^1\pi\pi^*/S_0$  CI is not known from these calculations. An insight into these branching ratios may be obtained using mixed quantum-classical dynamics simulations,<sup>13, 14</sup> however this method is considerably more involved.

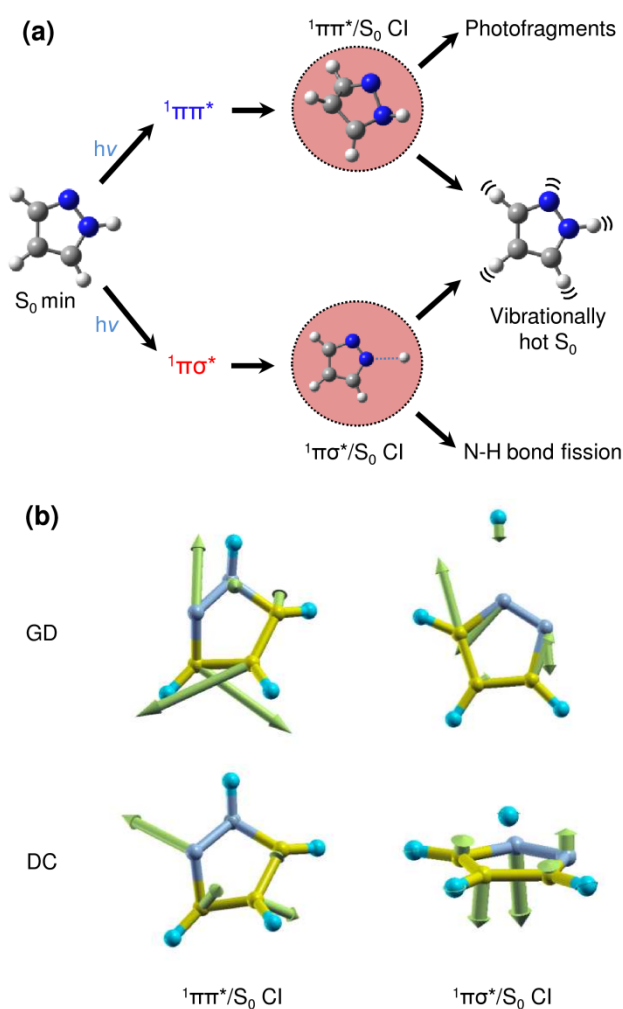


**Fig. S5** (a) Schematic of the possible molecular relaxation pathways available in pyrazole following excitation with 200 nm radiation,  $h\nu$ . Structures highlighted in red circles are calculated minimum energy crossing point (MECP) geometries for the  $^1\pi\pi^*/S_0$  and  $^1\pi\sigma^*/S_0$  conical intersections (CIs), at a CASSCF/6-31+G(d) level of theory. (b) Calculated gradient difference (GD) and derivative coupling (DC) branching space vectors for the  $^1\pi\pi^*/S_0$  and  $^1\pi\sigma^*/S_0$  CIs, which are responsible for lifting the electronic state degeneracy around the MECPs.

For completeness, we have also calculated the MECP geometry and branching space modes of the  ${}^1\pi\sigma^*/S_0$  CI, which occurs at elongated N-H distances ( $R_{N-H} = 2.14 \text{ \AA}$ ).<sup>6</sup> The geometry of this CI is labeled in Fig. S5(a) while the associated branching space vibrations are represented in Fig. S5(b). In imidazole, theory suggests that relaxation *via* a  ${}^1\pi\sigma^*/S_0$  CI is the dominant relaxation pathway following absorption of 200 nm radiation (~83 %),<sup>15</sup> and by analogy it is possible the same scenario will exist in pyrazole. As a result, we propose that population transfer to a vibrationally excited  $S_0$  state in both species is primarily mediated by these  ${}^1\pi\sigma^*/S_0$  CIs, rather than  ${}^1\pi\pi^*/S_0$  CIs.

---

## References

1. U. Even, J. Jortner, D. Noy, N. Lavie and C. Cossart-Magos, *J. Chem. Phys.*, 2000, **112**, 8068-8071.
2. A. T. J. B. Eppink and D. H. Parker, *Rev. Sci. Instrum.*, 1997, **68**, 3477-3484.
3. G. M. Roberts, J. L. Nixon, J. Lecointre, E. Wrede and J. R. R. Verlet, *Rev. Sci. Instrum.*, 2009, **80**, 053104.
4. J. D. Vaughan and W. A. Smith, *J. Am. Chem. Soc.*, 1972, **94**, 2460-2463.
5. D. J. Hadden, K. L. Wells, G. M. Roberts, L. T. Bergendahl, M. J. Paterson and V. G. Stavros, *Phys. Chem. Chem. Phys.*, 2011, **13**, 10342-10349.
6. C. A. Williams, G. M. Roberts, H. Yu, N. L. Evans, S. Ullrich and V. G. Stavros, *J. Phys. Chem. A*, 2011, DOI:10.1021/jp2053212.
7. K. A. Holbrook, M. J. Pilling and S. H. Robertson, *Unimolecular Reactions*, John Wiley and sons, Chichester, UK, 1996.
8. A. L. Devine, B. Cronin, M. G. D. Nix and M. N. R. Ashfold, *J. Chem. Phys.*, 2006, **125**, 184302.
9. G. A. King, T. A. A. Oliver, M. G. D. Nix and M. N. R. Ashfold, *J. Chem. Phys.*, 2010, **132**, 064305.
10. M. J. Frisch, G. W. Trucks, H. B. Schlegel, G. E. Scuseria, M. A. Robb, J. R. Cheeseman, J. A. Montgomery, Jr., T. Vreven, K. N. Kudin, J. C. Burant, J. M. Millam, S. S. Iyengar, J. Tomasi, V. Barone, B. Mennucci, M. Cossi, G. Scalmani, N. Rega, G. A. Petersson, H. Nakatsuji, M. Hada, M. Ehara, K. Toyota, R. Fukuda, J. Hasegawa, M. Ishida, T. Nakajima, Y. Honda, O. Kitao, H. Nakai, M. Klene, X. Li, J. E. Knox, H. P. Hratchian, J. B. Cross, V. Bakken, C. Adamo, J. Jaramillo, R. Gomperts, R. E. Stratmann, O. Yazyev, A. J. Austin, R. Cammi, C. Pomelli, J. W. Ochterski, P. Y. Ayala, K. Morokuma, G. A. Voth, P. Salvador, J. J. Dannenberg, V. G. Zakrzewski, S. Dapprich, A. D. Daniels, M. C. Strain, O. Farkas, D. K. Malick, A. D. Rabuck, K. Raghavachari, J. B. Foresman, J. V. Ortiz, Q. Cui, A. G. Baboul, S. Clifford, J. Cioslowski, B. B. Stefanov, G. Liu, A. Liashenko, P. Piskorz, I. Komaromi, R. L. Martin, D. J. Fox, T. Keith, M. A. Al-Laham, C. Y. Peng, A. Nanayakkara, M. Challacombe, P. M. W. Gill, B. Johnson, W. Chen, M. W. Wong, C. Gonzalez and J. A. Pople, *GAUSSIAN 03 (Revision D.01)*, Gaussian, Inc., Wallingford, CT, 2004.
11. M. Barbatti, H. Lischka, S. Salzmann and C. M. Marian, *J. Chem. Phys.*, 2009, **130**, 034305.
12. D. R. Yarkony, *Rev. Mod. Phys.*, 1996, **68**, 985-1013.
13. B. Sellner, M. Barbatti and H. Lischka, *J. Chem. Phys.*, 2009, **131**, 024312.
14. M. Vazdar, M. Eckert-Maksic, M. Barbatti and H. Lischka, *Mol. Phys.*, 2009, **107**, 845-854.
15. R. Crespo-Otero, M. Barbatti, H. Yu, N. L. Evans and S. Ullrich, *ChemPhysChem*, 2011, DOI:10.1002/cphc.201100453.